Surface-emitting terahertz quantum cascade lasers with continuous-wave power in the tens of milliwatt range

Gangyi Xu,[1,2,a)] Lianhe Li,[3] Nathalie Isac,[1] Yacine Halioua,[1] A. Giles Davies,[3] Edmund H. Linfield,[3] and Raffaele Colombelli[1,b)]
[1]*Institut d'Electronique Fondamentale, Univ. Paris Sud, UMR8622 CNRS, 91405 Orsay, France*
[2]*Key Laboratory of Infrared Imaging Materials and Detectors, Shanghai Institute of Technical Physics, Chinese Academy of Sciences, Shanghai 200083, China*
[3]*School of Electronic and Electrical Engineering, University of Leeds, Leeds LS9 2JT, United Kingdom*

(Received 14 November 2013; accepted 3 February 2014; published online 4 March 2014)

We demonstrate efficient surface-emitting terahertz frequency quantum cascade lasers with continuous wave output powers of 20–25 mW at 15 K and maximum operating temperatures of 80–85 K. The devices employ a resonant-phonon depopulation active region design with injector, and surface emission is realized using resonators based on graded photonic heterostructures (GPHs). GPHs can be regarded as energy wells for photons and have recently been implemented through grading the period of the photonic structure. In this paper, we show that it is possible to keep the period constant and grade instead the lateral metal coverage across the GPH. This strategy ensures spectrally single-mode operation across the whole laser dynamic range and represents an additional degree of freedom in the design of confining potentials for photons. © *2014 AIP Publishing LLC*.
[http://dx.doi.org/10.1063/1.4866661]

The ability to operate terahertz frequency quantum cascade lasers[1] (THz QCLs) in continuous-wave (CW) is essential for many applications, including their use in local oscillator systems,[2] spectroscopy/trace-gas detection,[3–6] and direct bolometric imaging.[7] It is also often important to ensure that the lasers have low dissipated power. Devices based on third-order distributed feedback (DFB) architectures are a good solution to these requirements,[8–10] since their dimensions can be scaled down without compromising the beam quality. But, for direct bolometric imaging, maximizing the emitted output power is also extremely important.[11]

In this Letter, we investigate device architectures that can provide high (tens of milliwatt) CW output powers. Specifically, we aim to obtain significantly higher powers than have been observed to date using either 2D photonic crystals[12–18] or second-order DFB gratings.[19–24] Recently, we have demonstrated surface-emitting THz QCLs based on graded photonic heterostructure (GPH) resonators (shown schematically in Fig. 1(a)).[25] Building on second-order DFB concepts, GPH resonators feature a graded periodicity of the metallic grating. In the original design,[25] the grating periodicity was symmetrically and gradually decreased from the center towards each end of the laser ridge. This resulted in an energy well for photons: the symmetric/radiative modes are spatially confined in the center of the grating and favored for lasing. The anti-symmetric/non-radiative modes—which have low power efficiency—are pushed towards the highly lossy device absorbing boundaries and are inactive. GPH lasers, therefore, exhibit stable single-mode emission with high power efficiency in pulsed mode, as well as naturally low-divergence single-lobed emission patterns.[25,26] The design of the GPH resonators must, however, be judiciously tailored to achieve stable single mode emission for all injected currents.[26]

We focus here on the CW, or quasi-CW, behavior of optimized GPH THz lasers and demonstrate output powers of more than 25 mW at 15 K and CW operation up to 82 K, with wall-plug efficiencies (WPE) in the range of 0.6%–0.7%. We also demonstrate an additional, very effective technique to implement GPH devices, in which the lateral metal coverage (i.e., the grating filling-factor) across the GPH is graded, rather than the periodicity (Fig. 1(a)). This allows one to increase stability of the single-mode emission from a device, without compromising its performance.

An intuitive picture of the two different GPH designs is given in Figs. 1(b) and 1(d). Fig. 1(b) shows the real-space photonic band diagram of a standard periodicity-graded GPH resonator.[25] The crucial feature is that the bands are always parallel. The detailed shape (e.g., linear or parabolic) depends on the recursive formula defining the grading of the periodicity. In this case, $\Delta a = a_i - a_{i+1} = 0.1\ \mu$m, where a_i is the periodicity of the i-th slit. This leads to an approximately linear potential, as Δa is much smaller than a_i. Since the photonic gap in these structures is quite narrow ($<10\%$ of the central frequency in our case), parallel photonic bands lead to a reduced flexibility to obtain, simultaneously, high output power and stable single mode emission over the whole laser dynamic range.

An alternative solution is to maintain a constant grating period, but vary the GPH filling-factor (ff), defined as the ratio of the metallic finger width to the period width (100% ff corresponds to full metallization; 0% ff to no metallization). This is because the frequency of the band-edge modes is not only determined by the periodicity but also significantly affected by the grating filling-factor. Figure 1(a) (lower) shows a device in which the ff decreases symmetrically and linearly from the center (95% ff) toward each end of the device (70% ff).

a)E-mail: gangyi.xu@mail.sitp.ac.cn
b)E-mail: raffaele.colombelli@u-psud.fr

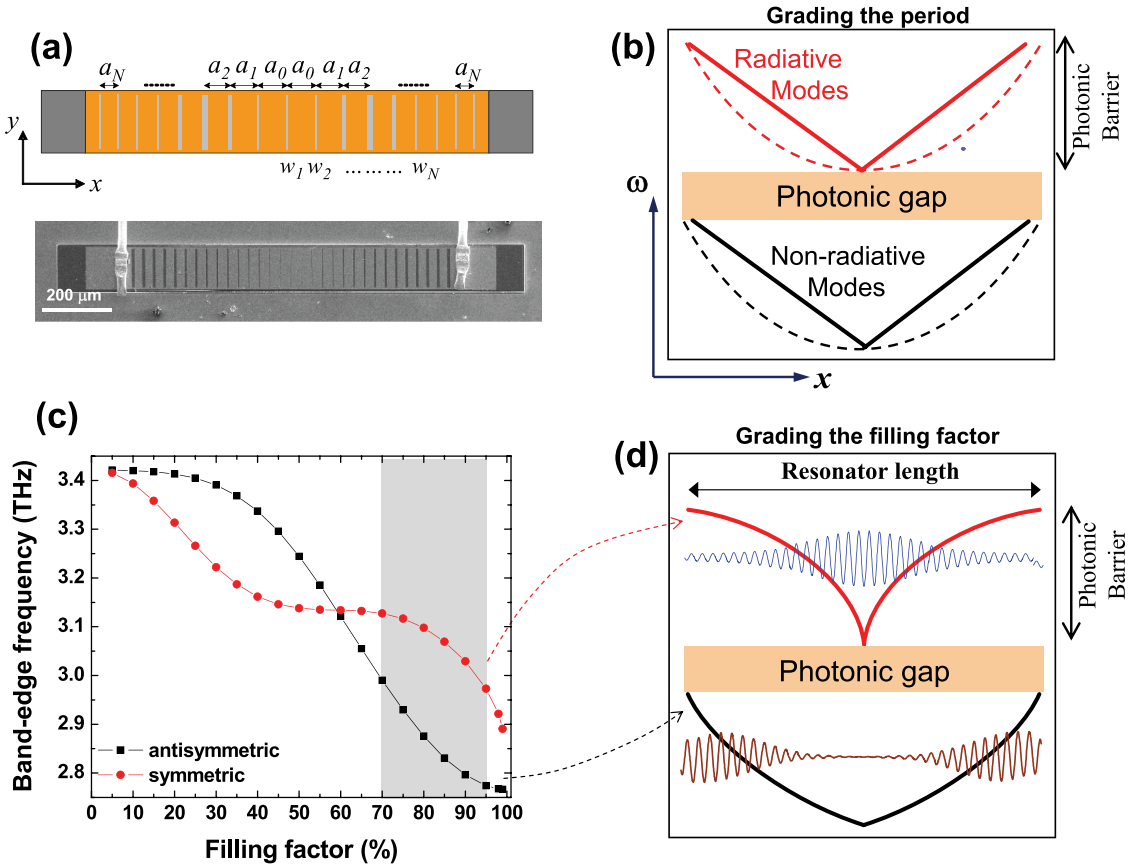

FIG. 1. (a) Two approaches are possible to implement a GPH resonator: grading of the grating periodicity or of the filling-factor. Upper: schematic diagram showing a GPH laser in which the periodicity a_i of the grating is graded. w_i is the width of the air slits. Lower: SEM picture of a GPH laser where the grating periodicity is constant, but the filling-factor of the upper metallization decreases symmetrically and linearly from the center toward each end of the ridge (i.e., the slit widths w_i increase from the center toward the end). (b) Real-space photonic band diagram of a periodicity-graded GPH resonator: the bands are parallel. The exact shape of the potential (linear—solid line; parabolic—dashed line) depends on the recursive formula used to grade the GPH period. (c) Eigen-frequencies of the two band-edge modes (at the zone center) as a function of the grating filling factor, for a grating structure with periodicity 30 μm. The black line with squares corresponds to the anti-symmetric mode; the red line with circles, the symmetric mode. (d) Real-space photonic band diagram of a filling-factor-graded GPH resonator, where the ff decreases linearly from 95% to 70%. Such a structure provides additional degrees of freedom in the design: it leads to a deep and sharp photonic well for the upper/symmetric mode, while a broad photonic barrier is experienced by the lower/anti-symmetric modes.

In order to understand intuitively the potential shape when the ff is varied, Fig. 1(c) shows the calculated frequency of the grating band-edge modes at the Γ-point as a function of ff, for a grating period $a_0 = 30\,\mu$m. The regions covered by the metallic fingers exhibit higher effective index than those without metal. As a result, the frequency of the band edge modes as a function of the ff is determined by the modal spatial distribution in the high/low effective index regions, respectively. Hence, decreasing the ff leads to an increase of the volume of the low-effective-index-region, which blue-shifts the frequency of both band edge modes. The light-grey highlighted zone in Fig. 1(c) corresponds to the ff range used in this work, which also best matches the device requirements, since very low filling-factors are incompatible with achieving uniform current injection.[27]

Based on Fig. 1(c), it is possible to infer the corresponding photonic-band diagram of the filling-factor-graded GPH (Fig. 1(d)). The photonic bands now have opposite curvatures. This provides additional design freedom: it leads to a deep and sharp photonic well for the symmetric/radiative modes, while a broad photonic barrier is experienced by the anti-symmetric modes. The consequence for laser operation is that it is easier to achieve single-mode spectra across the complete laser dynamic range.

THz QCLs with GPH resonators were fabricated using a GaAs resonant-phonon-depopulation active region design with an extended injector, as reported in Ref. 28 (wafer L773). This active region is very effective since it combines the advantages of resonant-phonon depopulation designs (high power and high maximum operation temperature T_{max}) with those based on bound-to-continuum designs (low threshold current). Ridge lasers from L773 operate in Au-Au double-metal waveguides up to a maximum temperature of 150 K in pulsed mode (105 K in CW), with low threshold (pulsed) current densities (J_{th}) of 160 Acm^{-2} and 370 Acm^{-2}, respectively, at 78 K and 150 K (data not shown). The emission frequency peaks at approximately 2.8 THz (approximately 107 μm).

We initially implemented a set of GPH THz lasers on L773 using the standard periodicity-graded design.[26] The value of Δa, the grading factor, was 100 nm, and a range of lasers with different initial a_0 values were fabricated. Typical spectral properties are reported in Fig. 2 for different a_0. At injected currents slightly above threshold, the lasers exhibit single mode emission and the wavelength correctly scales with the value of a_0 (Fig. 2(a)). Side-mode suppression ratios (SMSRs) of up to 30 dB are achieved (data not shown).

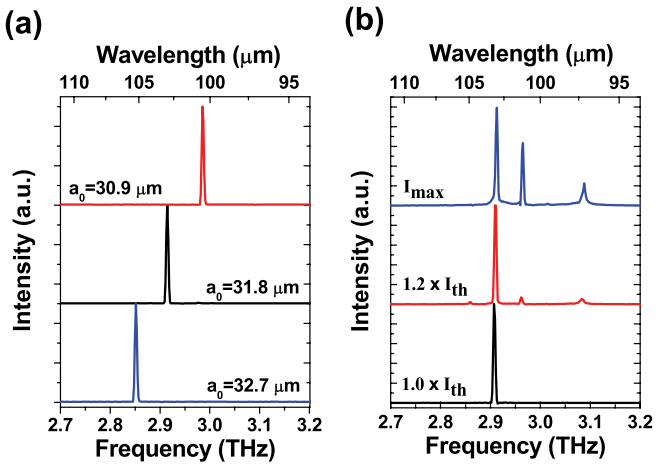

FIG. 2. (a) Emission spectra of periodicity-graded GPH lasers measured at 15 K with injection currents slightly above threshold. The lasers exhibit single-mode emission, and the wavelength scales approximately linearly with a_0, where a_0 is the periodicity of the central slit. (b) Emission spectra of a typical laser ($a_0 = 31.8\ \mu$m) measured at 15 K at different injected currents. As the operation current increases, weak side modes appear. They stem from the first-order antisymmetric (non-radiative) mode with lower frequency and the higher order symmetric (radiative) modes with higher frequencies, respectively.

However, as presented in Fig. 2(b), by increasing the operating current side modes appear. They stem from the first-order antisymmetric mode (non-radiative) and higher order symmetric modes (radiative), respectively.[26]

Figure 3(a) shows the calibrated *L-I-V* characteristics for a periodicity-graded GPH structure, measured with a Thomas Keating absolute THz power-meter in a quasi-CW regime (50% duty cycle at a repetition rate of 20 Hz, corresponding to pulses of 25 ms duration). More than 25 mW of output power is obtained at 15 K, with >10 mW still achieved at 60 K. This performance at 60 K is compatible with the use of small, compact Stirling-cycle cryocoolers; the WPE at 15 K is ~0.65%, at an operating bias of 10 V. It should be noted that, for the same device, we have also measured the average output power in both quasi-CW (20 Hz repetition rate, 50% duty cycle) and CW using a thermal power meter (OPHIR 3A-P-THz). The average output power scales linearly with the current duty cycle, thus confirming the high CW output power of GPH lasers. The emission is normal to the surface, and the corresponding angular pattern in the far-field is shown in Fig. 3(b). The far-field pattern is measured at 40 K with a current of about $1.1 \times I_{th}$ to ensure a single mode emission. As for all GPH THz surface-emitting lasers, the divergence angle of the output beam is diffraction limited. The elongated shape stems from the rectangular shape of the ridge resonator.

Figures 4 and 5 show the implementation, again on L773, of GPH structures based on the grading of the grating filling-factor. The emission frequency is once again lithographically tunable (Fig. 4(a)), but—in contrast to the previous design—it is now consistently single mode across the full dynamic range of the laser, as shown by Fig. 4(b). A very good SMSR of 35 dB is typically obtained (Fig. 4(c)). No device exhibited unwanted bi- or tri-modal emission. The far-field emission pattern was elongated once again, but no significant differences are seen between Figs. 3(b) and 5(b). The output power (Fig. 5(a)) was 20 mW in the quasi-CW regime at 15 K, with 12.5 mW achieved at 55 K. The T_{max} was 74 K, and the WPE of the filling-factor-graded GPH lasers was 0.6%. Note: the maximum output power reached with the filling-factor-graded laser is lower than that of the periodicity-graded laser. The main reason is that, at high current injection levels, the former maintains single mode emission whereas the latter exhibits bi- or tri-modal emission. Furthermore, as mentioned in the captions of Figs. 3(a) and 5(a), the device dimensions are slightly different.

In conclusion, THz GPH lasers have been realized, which operate CW and quasi-CW. They deliver tens of milliwatts output power, and have WPEs comparable to current state-of-the-art THz QCLs. The alternative GPH design presented in this work, in which the filling-factor rather than the

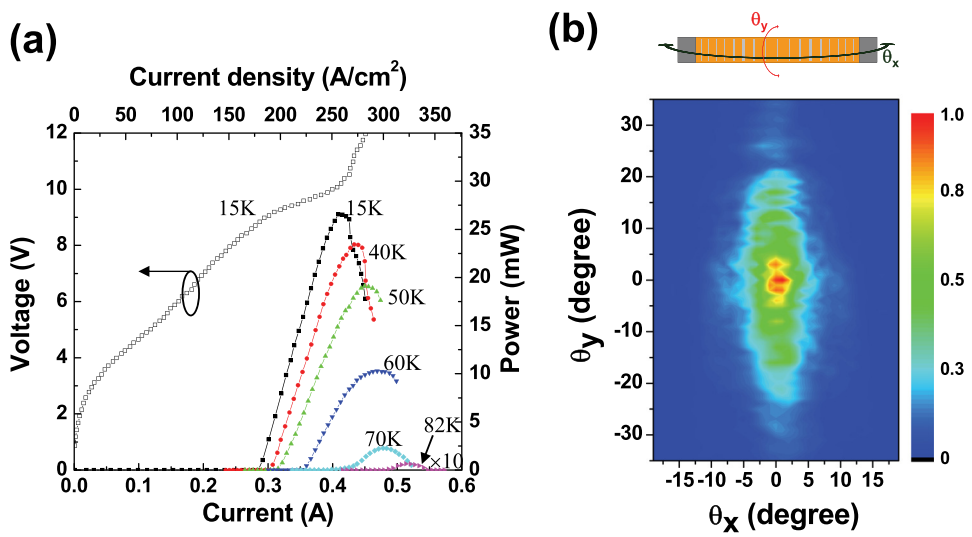

FIG. 3. (a) Light-current-voltage (*L-I-V*) characteristics of a typical periodicity-graded GPH laser ($a_0 = 31.8\ \mu$m) measured at different heat-sink temperatures. The output power is measured with a Thomas Keating absolute terahertz power-meter. The device was operated with 25 ms-long pulses, at a frequency of 20 Hz. The ridge width is 130 μm, and the number of periods is 39. The device dimensions are ~130 μm × 1180 μm. (b) Far-field emission pattern of the same device acquired at a heat-sink temperature of 40 K. The injected current is about $1.1 \times I_{th}$ to ensure single mode (the fundamental symmetric mode) emission. The measurement is performed by scanning a Golay cell on a spherical surface at a constant distance of ≈15 cm from the sample surface.

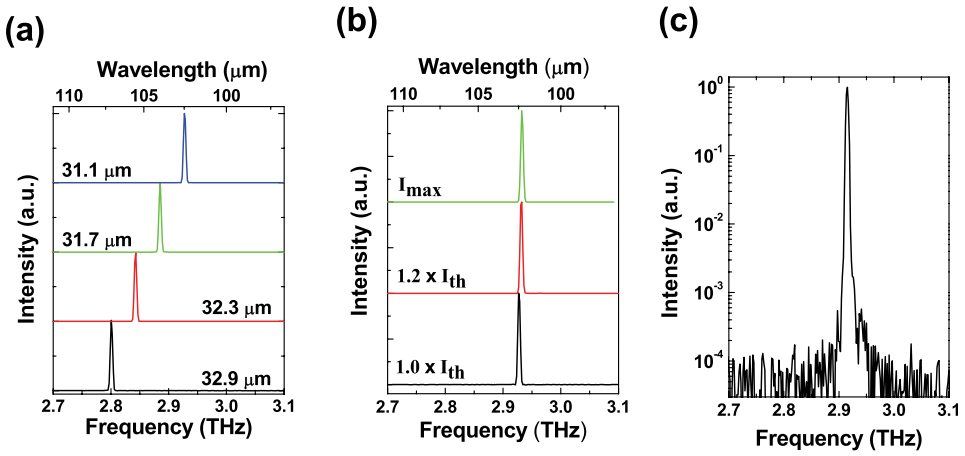

FIG. 4. (a) Emission spectra of filling-factor-graded GPH lasers measured at 15 K. The single-mode emission wavelength scales approximately linearly with the grating periodicity. (b) Emission spectra at different injection currents for a typical laser (grating periodicity 31.1 μm) measured at 15 K, demonstrating single mode emission across the whole dynamical ranges, from I_{th} up to I_{max}. (c) The side mode suppression ratio is typically ~30/35 dB (grating periodicity 31.1 μm). The measurement is performed at 40 K, at maximum output power.

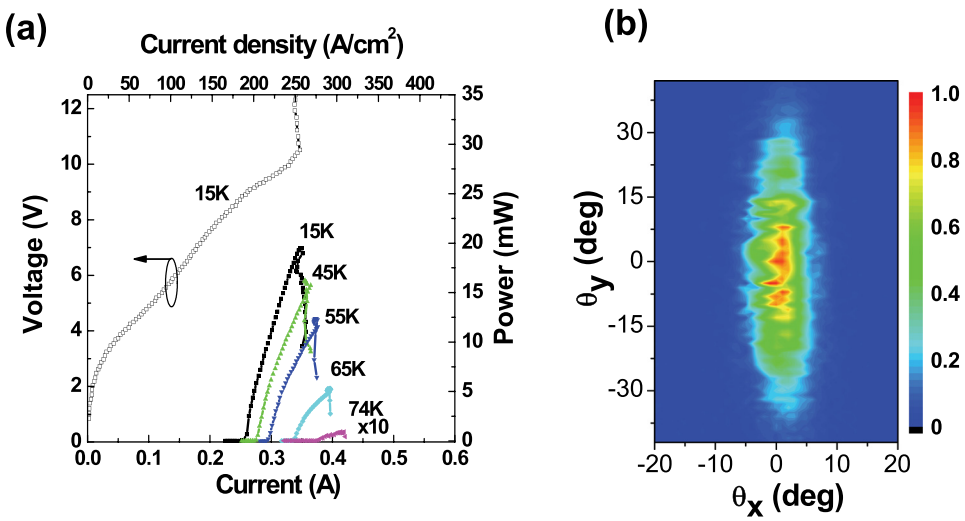

FIG. 5. (a) Light-current-voltage (*L-I-V*) characteristics of a typical filling-factor-graded GPH laser (grating periodicity 31.1 μm) measured at different heat-sink temperatures. The device was operated with 25 ms-long pulses, at a frequency of 20 Hz. The ridge width is 130 μm, and the number of periods is 33. The device dimensions are ~130 μm × 1020 μm. (b) Far-field emission pattern of the same device at a heat-sink temperature of 40 K.

periodicity is graded, shows stable single mode emission at all drive currents. Higher power and 2D Gaussian far-field patterns could be obtained by phase-locking arrays of optimized GPH devices.

We acknowledge support from the French National Research Agency (Nos. ANR-09-NANO-017 "Hi-Teq" and ANR-2011-NANO-020 "Delta"), and from the ERC "GEM" program. This work was partly supported by the French RENATECH network. Device fabrication was performed at the nano-center CTU-IEF-Minerve, which was partially funded by the Conseil Général de l'Essonne. The authors also acknowledge support from the EPSRC (UK), the ERC "NOTES" and "TOSCA" programmes, the Royal Society, and the Wolfson Foundation.

[1]R. Köhler, A. Tredicucci, F. Beltram, H. Beere, E. H. Linfield, A. G. Davies, D. A. Ritchie, R. C. Iotti, and F. Rossi, Nature **417**, 156 (2002).
[2]Y. Ren, D. J. Hayton, J. N. Hovenier, M. Cui, J. R. Gao, T. M. Klapwijk, S. C. Shi, Q. Hu, and J. L. Reno, Appl. Phys. Lett. **101**, 101111 (2012).
[3]M. Tonouchi, Nat. Photonics **1**, 97 (2007).
[4]B. S. Williams, Nat. Photonics **1**, 517 (2007).
[5]S. Borri, P. Patimisco, A. Sampaolo, H. E. Beere, D. A. Ritchie, M. S. Vitiello, G. Scamarcio, and V. Spagnolo, Appl. Phys. Lett. **103**, 021105 (2013).
[6]L. Consolino, S. Bartalini, H. E. Beere, D. A. Ritchie, M. S. Vitiello, and P. D. Natale, Sensors **13**, 3331 (2013).
[7]D.-T. Nguyen, F. Simoens, J. L. Ouvrier-Buffet, J. Meilhan, and J.-L. Coutaz, IEEE Trans. Terahertz Sci. Technol. **2**, 299 (2012).
[8]M. I. Amanti, G. Scalari, F. Castellano, M. Beck, and J. Faist, "Low divergence terahertz photonic-wire laser," Opt. Express **18**, 6390 (2010).
[9]M. I. Amanti, M. Fischer, G. Scalari, M. Beck, and J. Faist, Nat. Photonics **3**, 586 (2009).
[10]T.-Y. Kao, Q. Hu, and J. L. Reno, Opt. Lett. **37**, 2070 (2012).
[11]C. Sirtori, S. Barbieri, and R. Colombelli, Nat. Photonics **7**, 691 (2013).
[12]Y. Chassagneux, R. Colombelli, W. Maineult, S. Barbieri, H. Beere, D. Ritchie, S. P. Khanna, E. H. Linfield, and A. G. Davies, Nature **457**, 174–178 (2009).
[13]H. Zhang, G. Scalari, J. Faist, L. A. Dunbar, and R. Houdre, J. Appl. Phys. **108**, 093104 (2010).
[14]L. Sirigu, R. Terazzi, M. I. Amanti, M. Giovannini, J. Faist, L. A. Dunbar, and R. Houdré, Opt. Express **16**, 5206 (2008).
[15]Y. Chassagneux, R. Colombelli, W. Maineult, S. Barbieri, S. P. Khanna, E. H. Linfield, and A. G. Davies, Appl. Phys. Lett. **96**, 031104 (2010).
[16]Y. Chassagneux, Q. J. Wang, S. P. Khanna, E. Strupiechonski, J.-R. Coudevylle, E. H. Linfield, A. G. Davies, F. Capasso, M. Belkin, and R. Colombelli, IEEE Trans. Terahertz Sci. Technol. **2**, 83 (2012).
[17]G. Sevin, D. Fowler, G. Xu, F. H. Julien, R. Colombelli, S. P. Khanna, E. H. Linfield, and A. G. Davies, Appl. Phys. Lett. **97**, 131101 (2010).
[18]A. Benz, Ch. Deutsch, G. Fasching, K. Unterrainer, A. M. Andrews, P. Klang, W. Schrenk, and G. Strasser, Opt. Express **17**, 941 (2009).
[19]J. A. Fan, M. A. Belkin, F. Capasso, S. Khanna, M. Lachab, A. G. Davies, and E. H. Linfield, Opt. Express **14**, 11672 (2006).
[20]S. Kumar, B. S. Williams, Q. Qin, A. W. M. Lee, and Q. Hu, Opt. Express **15**, 113 (2007).
[21]L. Mahler, A. Tredicucci, F. Beltram, C. Walther, H. E. Beere, and D. A. Ritchie, Opt. Express **17**, 6703 (2009).
[22]L. Mahler, A. Tredicucci, F. Beltram, C. Walther, J. Faist, B. Witzigmann, H. E. Beere, and D. A. Ritchie, Nat. Photonics **3**, 46 (2009).
[23]E. Mujagic, C. Deutsch, H. Detz, P. Klang, M. Nobile, A. M. Andrews, W. Schrenk, K. Unterrainer, and G. Strasser, Appl. Phys. Lett. **95**, 011120 (2009).

[24]L. Mahler, A. Tredicucci, F. Beltram, C. Walther, J. Faist, H. E. Beere, and D. A. Ritchie, Appl. Phys. Lett. **96**, 191109 (2010).
[25]G. Xu, R. Colombelli, S. P. Khanna, A. Belarouci, X. Letartre, L. Li, E. H. Linfield, A. G. Davies, H. E. Beere, and D. A. Ritchie, Nat. Commun. **3**, 952 (2012).
[26]G. Xu, Y. Halioua, S. Moumdji, R. Colombelli, H. E. Beere, and D. A. Ritchie, Appl. Phys. Lett. **102**, 231105 (2013).
[27]Note that DC values larger than 60% must be used since below that value there is an inversion: The radiative mode is located at a lower frequency with respect to the non-radiative mode, and the structure would need to be re-designed.
[28]M. I. Amanti, G. Scalari, R. Terazzi, M. Fischer, M. Beck, J. Faist, A. Rudra, P. Gallo, and E. Kapon, New J. Phys. **11**, 125022 (2009).